Two-color laser absorption near 5 μm for temperature and nitric oxide sensing in high-temperature gases

Christopher A. Almodovar[a,*], R. Mitchell Spearrin[b], Ronald K. Hanson[a]

[a] *High Temperature Gas Dynamics Laboratory, Department of Mechanical Engineering, Stanford University, Stanford, CA 94305, USA*
[b] *Mechanical and Aerospace Engineering Department, University of California Los Angeles (UCLA), Los Angeles, CA 90095, USA*

Abstract

An infrared laser-absorption technique for *in situ* temperature and nitric oxide species sensing in high-temperature gases is presented. A pair of quantum cascade lasers in the mid-infrared near 5 μm were utilized to probe rovibrational transitions in nitric oxide's fundamental band. The line parameters of the selected transitions, including line strengths and collision broadening coefficients of nitric oxide with argon and nitrogen, were evaluated during controlled room-temperature static cell experiments and high-temperature shock tube experiments at temperatures between 1000 and 3000 K, and pressures between 1 and 5 atm. These studies provided new insights into the temperature dependence of nitric oxide collision broadening, highlighting the inadequacies of the power law over a broad temperature range. With an accurate spectroscopic model over a broad temperature range, the quantitative two-color temperature sensing strategy was demonstrated in non-reactive shock tube experiments from 1000 to 3000 K to validate thermometry and during a nitric oxide formation experiment near 1700 K and 4 atm to highlight capability for temporally-resolved species measurements at MHz rates. The technique has applicability for sensing in a broad range of flow fields that involve high-temperature air.

Keywords: Nitric oxide, Laser absorption, Spectroscopy, Mid-infrared, High temperature, Quantum cascade laser

1. Introduction

Nitric oxide (NO) forms in heated air or combustion exhaust gases by the oxidation of nitrogen which is described by the Zeldovich mechanism [1]. The extent of its formation is strongly coupled with temperature as equilibrium calculations of dry air show that the mole fraction of NO quickly grows from 200 ppm at 1200 K to 4% at 3000 K, at atmospheric pressure. The effects of high-temperature NO formation from combustion engines can be seen in the photochemical smog that hovers above urban areas [2]. Despite being unwanted due to environmental concerns, nitric oxide's increased presence at elevated temperatures can be exploited to measure gas properties with absorption spectroscopy. This paper presents a novel sensing strategy for measurement of temperature and NO mole fraction at high-enthalpy air conditions (1000-3000 K).

The desire to accurately monitor NO and processes that produce it is demonstrated by the body of work focused on NO absorption spectroscopy, particularly in its fundamental vibration band. Interest in using mid-IR absorption spectroscopy for remote sensing of NO in the atmosphere has motivated many spectroscopic studies of the fundamental vibration band at temperatures between 200 and 300 K. These studies, typically performed with Fourier transform absorption spectroscopy, focused on wide surveys of the fundamental band to improve or provide reassurance for previously measured or calculated values of spectroscopic parameters such as line positions, line strengths, collision broadening coefficients, and collision-induced line shifts. With a continually improving spectroscopic database, atmospheric scientists are able to take meaningful measurements of NO and better understand its role in atmospheric processes [4–8]. More relevant to the current

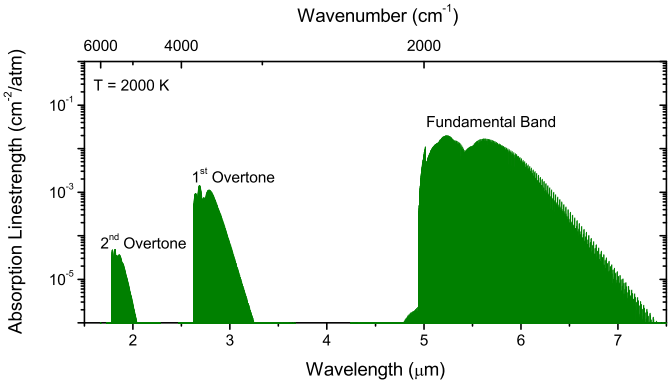

Fig. 1: Absorption linestrengths (HITEMP 2010) of the infrared NO spectrum at 2000 K and 1 atm [3].

*Correspondence to 452 Escondido Mall, Bldg. 520, Stanford, CA 94305

Email addresses: calmod@stanford.edu (Christopher A. Almodovar), spearrin@ucla.edu (R. Mitchell Spearrin), rkhanson@stanford.edu (Ronald K. Hanson)

work, is the use of NO spectroscopy in high-temperature gas sensing (> 1000 K), which has received less attention with regards to spectroscopic investigation. In this work, access to the fundamental vibration band of the NO spectrum is particularly attractive due to strong signals at the conditions of interest as shown in Fig. 1.

Heated air, which involves the formation of NO, is utilized in many applications such as power generation from combustion and in propulsion ground test facilities where preheaters heat and pressurize air before expanding it to supersonic conditions [9]. Recently, Spearrin *et al.* developed a method to measure temperature in high-enthalpy air flows with a continuous wave (CW) external cavity quantum cascade laser. The method measures the NO concentration via absorption spectroscopy at a wavelength near the $^2\Pi_{3/2}R(15.5)(v = 1 \leftarrow 0)$ transition of the fundamental band and uses the strong temperature dependence of NO concentration in equilibrium air to infer temperature [10]. Furthermore, absorption spectroscopy of the fundamental band of NO has been used to measure velocity, temperature, and NO concentration in the test section of a high-enthalpy hypersonic wind tunnel [11]. Other high-temperature applications of NO absorption spectroscopy can be found in combustion and chemical kinetic studies. An early utilization of the fundamental band for high-temperature NO sensing in shock tubes was demonstrated by Hanson *et al.* at a fixed wavelength near the $^2\Pi_{3/2}$ R(18.5) transition using a grating-tunable carbon monoxide (CO) laser [12]. Falcone *et al.* extended high-temperature sensing of NO by studying numerous rovibrational transitions (P(2.5)–R(14.5)) in the fundamental band using a low-power ($< 100\mu W$), cryogenic diode laser system. Line shape profiles in nitrogen, argon, and combustion gases were characterized for use in kinetic shock tube and combustion studies [13, 14]. In a similar manner, von Gersum and Roth used cryogenically-cooled diode lasers, probing the P(6.5), P(11.5) and R(21.5) transitions of the $^2\Pi_{1/2}$ subband to study the decomposition of NO in argon (Ar) behind shock waves over a temperature range of 2500–3500 K [15]. More recently, the emergence of room-temperature, high-power, tunable quantum cascade lasers has allowed field demonstrations of NO sensing in combustion gases from a coal-fired power plant [16] and in analyzing exhaled human breath for respiratory issues [17]. Additionally, a number of infrared LAS-based sensors for NO using the first and second overtone bands have been designed and demonstrated [18, 19].

The current study advances upon the work of Spearrin *et al.* by developing a sensor for high-temperature gases that measures temperature under both chemical equilibrium and non-equilibrium conditions (e.g. situations when residence times are short) when appreciable concentrations of NO are present. Of note is a new wavelength-pairing selected for sensing in non-equilibrium conditions. Here, we present the design and development of a new multi-wavelength temperature- and species-sensing strategy, the measurement of requisite fundamental spectroscopic parameters of NO near 5 μm, and the demonstration of temperature and NO sensing using the proposed sensor in a shock tube. Absorption transitions in the fundamental absorption band of NO were selected because of their strong signals (1 to 2 orders of magnitude stronger than the 1st and 2nd overtone bands; see Fig.1) over the range of conditions studied here and because they can be accessed via commercially available, tunable quantum cascade lasers. Two quantum cascade lasers were used to measure four rovibrational transitions in a variety of conditions during static cell and shock tube experiments. To the knowledge of the authors, no spectroscopic measurements of the selected transitions have been made at elevated temperatures as presented here. The spectroscopic parameters were measured assuming Voigt line shape profiles over a range of temperatures and pressures. Lastly, the sensor's capabilities were demonstrated under non-reactive and reactive conditions in a shock tube.

2. Laser Absorption Spectroscopy and Line Selection

Laser absorption spectroscopy (LAS) is a well-known gas-sensing technique that has been effectively demonstrated in many high-temperature applications [20]. An accurate spectroscopic database and model is needed for quantitative temperature and species measurements. Key spectroscopic parameters can be determined experimentally by measuring the amount of light transmitted through a well-known thermodynamic environment and applying the Beer-Lambert relation for monochromatic light at frequency ν

$$-ln\left(\frac{I_t}{I_0}\right)_\nu = \alpha_\nu = \sum_i PX_{abs}S_i(T)\Phi_i(\nu)L \qquad (1)$$

where I_t/I_0 is the ratio of transmitted to incident light intensity, α_ν is the absorbance at frequency ν, P is pressure (atm), X_{abs} is the mole fraction of the absorbing species, $S_i(T)$ ($\mathrm{cm^{-2}atm^{-1}}$) is the temperature-dependent line strength of the quantum transition i, $\Phi_i(\nu)$ (cm) is the line shape function of the quantum transition i, and L (cm) is the uniform path length over which light is absorbed [21]. Of interest to the measurements presented here include the line strength and line shape profiles of the selected transitions. Tabulated spectroscopic parameters – line position, line strength, lower state energy, pressure broadening coefficients, pressure induced line shift, and temperature-dependence exponents – can be found in databases such as HITEMP 2010 [3]. However, at very high temperatures and high lower-state rotational quantum numbers (J") the database is often inadequate for accurate gas sensing. Nevertheless, these databases are an essential starting point for simulations and sensor line selection.

Fig. 2 shows a simulation of the absorbance spectrum of NO in air. The R-branch is simulated from 1920 to 2000

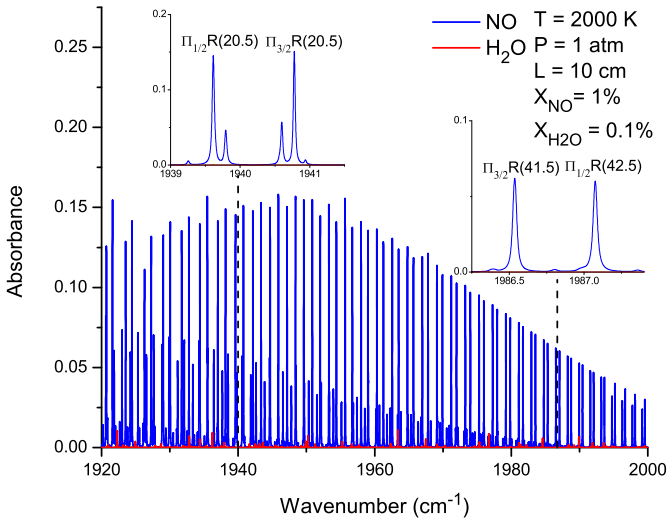

Fig. 2: Simulated absorbance spectrum (HITEMP 2010) of NO in air at 1 atm, 2000 K, and X_{NO} fixed at 1%. Water Vapor is also simulated at 1 atm, 2000 K and 1000 ppm.

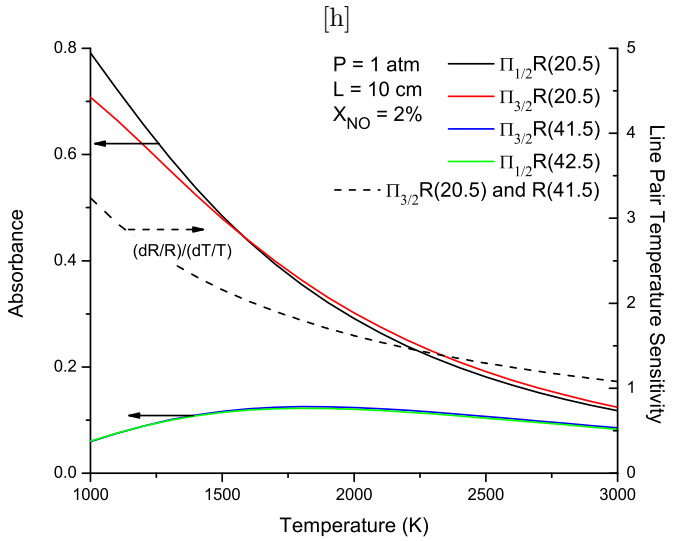

Fig. 3: Absorbance and temperature sensitivity of the selected transitions at fixed pressure and NO mole fraction.

cm^{-1} at 1 atm, 2000 K, and 1% NO in air. The water spectrum was also simulated at 2000 K for a concentration of 1000 ppm. Four transitions were selected to minimize water interference while maintaining a large lower state energy difference ($\Delta E''$) between line pairs, which is essential for sensitive temperature diagnostics (see temperature sensitivity discussion below). The insets of Fig. 2 show simulations of the studied transitions, namely the R(20.5) transitions of the $X^2\Pi_{1/2}$ and $X^2\Pi_{3/2}$ subbands of the electronic ground state and the $X^2\Pi_{3/2}$ R(41.5) and $X^2\Pi_{1/2}$ R(42.5) transitions.

Absorbance at transition line centers is simulated versus temperature in Fig. 3 for fixed pressure (1 atm) and 2 % NO mole fraction in air. The two R(20.5) transitions show strong variations in absorbance over the entire temperature range while the R(41.5) and R(42.5) transitions (slightly overlapped in Fig. 3) show less drastic changes. The behavior of these transitions with respect to temperature is advantageous for temperature sensing. Several demonstrations of two-transition temperature measurements have been reported throughout the literature beginning with [22]. These methods utilize the integrated absorbance (A_i) of a quantum transition, defined by [21]:

$$A_i = \int_{-\infty}^{\infty} \alpha(\nu) d\nu = P X_{abs} S_i(T) L \tag{2}$$

For a single absorbing species, a ratio of integrated absorbances is a function of only line strengths and thus temperature.

$$R(T) = \frac{A_1}{A_2} = \frac{S_1(T)}{S_2(T)} \tag{3}$$

The transition line strength's relation to temperature can be expressed as

$$S_i(T) = S_i(T_0)\frac{Q(T_0)}{Q(T)}\left(\frac{T_0}{T}\right)\exp\left[-\frac{hcE_i"}{k}\left(\frac{1}{T}-\frac{1}{T_0}\right)\right]\times \left[1-exp\left(\frac{-hc\nu_{0,i}}{kT}\right)\right]\left[1-exp\left(\frac{-hc\nu_{0,i}}{kT_0}\right)\right]^{-1} \tag{4}$$

where T_0 is a reference temperature (typically 296 K), Q is the partition function of the absorbing species, h is Planck's constant, c is the speed of light, k is Boltzmann's constant, E" is the lower state energy of the transition, and $\nu_{0,i}$ is the line center frequency of transition i [21]. Taking the derivative of the ratio of integrated areas with respect to temperature and normalizing gives the normalized temperature sensitivity

$$\frac{dR/R}{dT/T} \approx \left(\frac{hc}{k}\right)\frac{(E_1" - E_2")}{T} = \left(\frac{hc}{k}\right)\frac{\Delta E"}{T} \tag{5}$$

Hence when employing this method, it is ideal to select transitions with a large ΔE". This technique requires full or nearly full resolution of the transition's line shape profile $\Phi_i(\nu)$, often achieved via tunable diode lasers. However, at elevated pressures, individual line shapes are no longer resolvable which requires further spectroscopic characterization. From Eq. (1), a ratio of absorbances is not only a function of line strengths but also of transition line shape functions. The Voigt line shape function is commonly used in molecular spectroscopy and is dependent on the collision and Doppler broadening of the gas mixture. The collision-dependent full-width at half-maximum (FWHM) is defined by

$$\Delta\nu_c = P\sum_A X_A 2\gamma_{B-A} \tag{6}$$

where $2\gamma_{B-A}$ is the FWHM collision broadening coefficient of absorbing molecule B with collision partner A

[21]. From Eq. (6), the addition of line shape profiles to the absorbance ratio requires knowledge of the collision broadening coefficients of the absorbing species with its collision partners. Therefore, study of collision broadening parameters over a wide temperature range is essential for development of an accurate LAS-based sensor for applications where the full line shape profile cannot be resolved (e.g. high-pressure environments). The temperature dependence of the collision broadening coefficient is often modeled with the power-law expression

$$2\gamma(T) = 2\gamma(T_0)\left(\frac{T_0}{T}\right)^n \tag{7}$$

where n is the temperature dependence exponent and $2\gamma(T_0)$ is the collisional broadening coefficient at the reference temperature, T_0, which is usually 296 K [21].

3. Experimental Setup

Two facilities were utilized to measure line strengths and collision widths in a variety of gas conditions: a room-temperature static cell and a stainless steel shock tube. Pressure in the 21 cm long static cell was measured with an MKS Baratron capacitance manometer pressure transducer (resolution to 1 torr). The 15.4 cm inner diameter stainless steel shock tube, with a 3.7 m long driver section and a 10 m long driven section, was used to achieve a variety of conditions between 1000 – 3000 K and 1 – 5 atm. Before each shock tube experiment, driven and driver sections were separated by a thin plastic diaphragm, both sections were evacuated, and the driven section was filled with the test gas (i.e. 1.97% NO in N_2 or 2% NO in Ar). The shock wave was generated by filling the driver section with helium until the diaphragm ruptured. The diaphragm rupture was controlled by a two-blade, perpendicular cutting device for diaphragms up to 0.020" and by scores in thicker diaphragms (0.040" and 0.060"). Test conditions were determined by measuring the incident shock speed via a series of five piezoelectric pressure transducers over the last 1.5 m of the driven section. The five transducers triggered time-interval counters (Fluke PM6666) from which the incident shock speed was extrapolated to the end wall where the normal shock jump relations were used to determine thermodynamic conditions behind the reflected shock. The measurement location was located two centimeters from the end wall where optical access ports and a Kistler 603B1 pressure gauge were positioned.

By careful measurement of the pre-shock conditions and incident shock speed, the thermodynamic conditions behind the reflected shock can be known to within $\sim 1\%$ [23]. Furthermore, Farooq *et al.* and Spearrin *et al.* demonstrated the agreement between measured and calculated (via the normal shock relations) temperatures behind the reflected shock in non-reactive shock tube experiments of CO_2 balanced in Ar [24, 25]. Also worth considering as a contributor to uncertainty in LAS temperature measurements in shock tubes is boundary layer development. Since

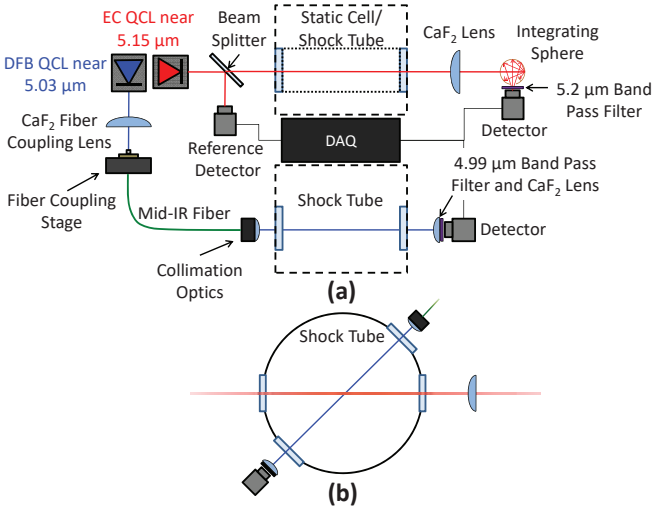

Fig. 4: Experiment Setup. Panel (a) shows the instrumentation and equipment for static cell and/or shock tube experiments; (b) shows the line of sights during shock tube experiments.

LAS is a line of sight measurement, cool gas in a relatively thick boundary layer may introduce inaccuracies to the measurement, especially in small diameter shock tubes and if low E" transitions are involved. Over the years, several models for boundary layer growth in shock tubes have been developed, beginning with the work by Mirels [26]. For the experimental conditions of interest here, numerical simulations [27] show that the maximum boundary layer thickness is on the order of 1 mm which is a small fraction of the 15.24 cm inner diameter of the shock tube.

Two quantum cascade lasers were used to measure the spectral properties of the selected transitions. A diagram of the experimental setup is shown in Fig. 4. First, a Daylight Solutions external cavity quantum cascade laser (ECQCL) probed the transitions near 1940 cm^{-1}. Before entering the test cell, the ECQCL beam was split using a 2-degree wedged CaF_2 window. The reflected beam was diverted to a reference detector that was used to improve signal quality via common-mode rejection [28]. After passing through the cell, the transmitted beam was collected by a detection system consisting of a 10 cm focal-length CaF_2 plano-convex lens, a baffled 2.54 cm diameter integrating sphere with 6.35 mm ports, a 5.2 μm band pass filter, and a liquid nitrogen cooled indium-antimonide detector (2 mm diameter; 1 MHz bandwidth) from Infrared Associates, Inc. The gold-coated integrating sphere (Labsphere) decreases sensitivity to beam steering due to density gradients in the shock tube. Light entering the integrating sphere is diffusely reflected, which results in homogeneous light intensity at the ports [10, 29]. During shock tube experiments, the ECQCL could not be modulated rapidly enough to fully resolve transition line shape profiles, so the wavelength was monitored with a Bristol wavelength meter for fixed-wavelength measurements.

The second laser is an Alpes distributed feedback quan-

tum cascade laser (DFBQCL) that measured the transitions near 1987 cm^{-1}. As a way to spatially filter the TEM_{10} Hermite-Gaussian spatial mode of the DFBQCL, the beam was fiber-coupled to a tapered hollow core fiber (from Opto-Knowledge Systems, Inc.) with an inner diameter varying from 200-to-275 μm [30, 31]. The beam was fiber-coupled to the fiber using a 40 mm focal length infrared anti-reflection coated plano-convex lens and a 3-axis fiber-coupling stage. Once through the fiber, a 5 cm focal length plano-convex lens was used to collimate the beam through the shock tube and to the 25.4 mm focal length collection lens where the light was focused through the 4.9 μm band pass filter and onto a Vigo thermoelectrically cooled mercury cadmium telluride detector (2mm x 2mm area; 10 MHz bandwidth). For experiments where the output wavelength was modulated, a solid germanium Fabry-Perot etalon (FSR = 0.0566 cm^{-1}) was used to calibrate the relative output wavelength.

4. Spectroscopic Measurements

Important spectroscopic parameters are tabulated in databases such as HITRAN [32] and HITEMP, however, for high J" quantum numbers and very high temperatures, these databases are often inadequate due to a lack of experimental investigation and breakdown in the power-law over a wide-temperature range. For the transitions under investigation, HITRAN and HITEMP tabulate identical spectroscopic parameter values. The line strength uncertainties are cited to be between 5 and 10 % while the uncertainties in collision broadening coefficients in air at 1500 K for the R(20.5) transitions propagate to 12.5–25 % and collision broadening coefficients of the R(41.5) and R(42.5) transitions at elevated temperatures are cited as averages or estimates [3]. Additionally, for J" $>$ 16.5 the listed collision broadening temperature exponent values are assumed to be 0.6 and 0.7 for $\Pi_{1/2}$ and $\Pi_{3/2}$ respectively [33]. Quantitative measurements of either temperature or NO concentration require a more refined spectroscopic model. Thus, measurements in a controlled environment were made to either validate or improve database values. Furthermore, the HITRAN databases do not include collision broadening parameters for species in Ar, which is commonly used as a bath gas in combustion studies, so measurements of collision broadening in Ar were made in addition to measurements in N_2. The results of such measurements are presented here. First, room temperature measurements of NO spectra in N_2 were conducted in the static cell. The results of these measurements are used to determine if the Voigt profile adequately models the measured spectra and to validate the HITEMP line strength and room-temperature collision broadening. Next, high-temperature shock tube experiments were used to characterize the high-temperature spectra of NO in N_2 and Ar. Again, the validity of using the Voigt profile was investigated along with validation of the HITEMP line strengths and the characterization of the collision broadening coefficients and their temperature dependence from 1000-3000 K, which is essential for accurate gas sensing over this temperature range.

Static cell experiments were conducted over a range of gas densities to test the Voigt lineshape model. The room temperature static cell was filled with 1.01% NO in N_2, and the ECQCL's piezoelectric controller was driven by a 50 Hz sine wave which tuned the laser over the $\Pi_{1/2}$ R(20.5) and $\Pi_{3/2}$ R(20.5) transitions to resolve the absorbance profile as shown in the left panel of Fig. 5. Using a non-linear least squares fitting algorithm, the measured absorbance profiles were fit to Voigt profiles with the line center frequency, ν_0, the collision FWHM, $\Delta\nu_c$, and the integrated absorbance, A, as the best-fit parameters. Despite the evident lambda-doubling of NO spectra at low pressures, a single Voigt profile fit at moderate pressures accurately captures the measured absorbance profiles as shown in the peak-normalized residuals ($\sim$ 1%) of Fig 5. Using Eqs. (2) and (6), line strength and collision broadening coefficients can be calculated from the best-fit parameters $\Delta\nu_c$ and A_i. With room-temperature information, direct comparisons with values in HITEMP can be made. Measured lines strengths for the R(20.5) transitions differed from HITEMP values by 1.3 and 1%, and the measured collision broadening coefficients differed by 5%. Differences in collision broadening coefficients can be attributed to the fact that HITEMP reports $2\gamma_{NO-Air}$ which is smaller than the present value, likely because $2\gamma_{NO-O_2}$ is $\sim$ 17% smaller than broadening in N_2 [34]. Moreover, Spencer *et al.*'s measurements of the R(20.5) $2\gamma_{NO-N_2}(T = 296K)$ differ from the present measurements by less than 1% [6]. Ideally, similar room-temperature experiments would be performed for the $\Pi_{3/2}$ R(41.5) and $\Pi_{1/2}$ R(42.5) transitions. However, the high lower-state energies of these transitions render them unobservable with the experimental path length and room temperature conditions of our static cell. Therefore, high-temperature shock tube experiments were used to characterize the spectra of these transitions.

Shock tube experiments were performed over conditions between 1000–3000 K and 1–5 atm with the test gases being either 1.97 % NO in nitrogen or 2 % NO in argon. Unlike the room-temperature static cell measurements, the ECQCL cannot be tuned rapidly enough to fully resolve transition line shape profiles during shock tube experiments. Therefore, fixed-wavelength direct absorption (DA) experiments were performed with the ECQCL set near the peak of the $\Pi_{3/2}$ R(20.5) transition (1940.778 cm^{-1}). In the fixed-DA experiments, line shape properties were inferred from the measured line center absorbance of NO assuming the Voigt lineshape function. Given the known temperature and pressure of the shock tube experiments, absorbance simulations were altered by scaling the broadening coefficient of the $\Pi_{3/2}$ R(20.5) transition until the simulated and measured absorbances matched. The left and right panels of Fig. 6 show results for exper-

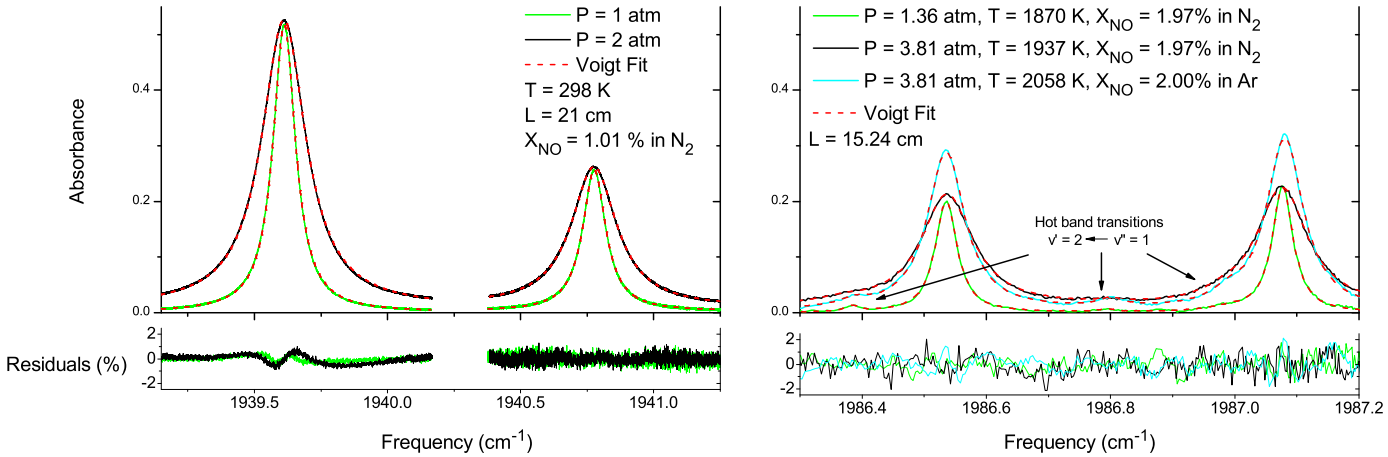

Fig. 5: The left panel displays Voigt fits to measured line shapes of the $\Pi_{1/2}$ R(20.5) and $\Pi_{3/2}$ R(20.5) transitions of nitric oxide's fundamental band; measurements were made in a room-temperature static cell. The right panel displays Voigt fits to measured line shapes of the $\Pi_{3/2}$ R(41.5) and $\Pi_{1/2}$ R(42.5) transitions; measurements were made during shock tube experiments.

Table 1: Summary and comparison of measured line strengths with HITEMP 2010. Uncertainties are given in parenthesis. Line center frequency and lower state energy are averages of the hyperfine lambda-doubled pairs and line strengths are the sum of the hyperfine lambda-doubled pairs.

ν_0 [cm^{-1}]	E" [cm^{-1}]	Transition			S_i(296 K) [cm^{-2}/atm]	
		Spin Split	$v' \leftarrow v$"	$j' \leftarrow j$"	Measured	HITEMP 2010
1939.614	735.468	$\Pi_{1/2}$	$1 \leftarrow 0$	R(20.5)	0.378 (2.5%)	0.373 (5-10%)
1940.778	874.735	$\Pi_{3/2}$	$1 \leftarrow 0$	R(20.5)	0.191 (2.5%)	0.189 (5-10%)
1986.537	3125.621	$\Pi_{3/2}$	$1 \leftarrow 0$	R(41.5)	6.73E-6 (1%)	6.74E-6 (5-10%)
1987.074	3081.772	$\Pi_{1/2}$	$1 \leftarrow 0$	R(42.5)	8.65E-6 (1%)	8.54E-6 (5-10%)

iments in argon and nitrogen, respectively. As mentioned previously, the temperature dependence of the collision broadening coefficients is typically modeled by a power-law function (Eq. (7)). Over the temperature range of 1000 to 3000 K, the best-fit temperature exponents of the collision broadening coefficient for the $\Pi_{3/2}R(20.5)$ transition were found to be $n = 0.56$ and $n = 0.55$ for argon and nitrogen, respectively. As expected, broadening due to argon was found to be less than broadening due to N_2. The collision broadening coefficient, $2\gamma_{B-A}$, is proportional to $\sigma^2_{A-B}/(\mu_{A-B})^{1/2}$ where σ_{A-B} and μ_{A-B} are the optical collision diameter and reduced mass of molecules A and B, respectively [21]. Thus, broadening due to nitrogen is larger because nitrogen has a larger effective optical diameter and is lighter than argon. From the power-law fit, the best-fit $2\gamma_{NO-Ar}(T_0 = 1000K) = 0.0331$ cm^{-1}/atm and $2\gamma_{NO-N_2}(T_0 = 1000K) = 0.0475$ cm^{-1}/atm, which differs from the HITEMP value by 10%. The collision broadening data was also fit with $T_0 = 296K$ which resulted in $2\gamma_{NO-N_2}(T_0 = 296K) = 0.0929$ cm^{-1}/atm, which underpredicts both HITEMP 2010 and the measurements made in the room-temperature static cell by 6 and 11 %, respectively. This discrepancy is likely due to inadequacies in Eq. (7) over large temperature ranges that have been discussed in collision broadening studies of CO and CO_2 [35–37]. As a result, caution should be made when using the data presented here outside of the studied temperature range or when extrapolating from low-temperature data.

The DFBQCL was operated to perform scanned-DA measurements during the shock tube experiments. The laser is capable of rapid tuning that allowed the entire line shape profiles of the $\Pi_{3/2}$ R(41.5) and $\Pi_{1/2}$ R(42.5) transitions to be resolved as shown in the right panel of Fig. 5. During these experiments, the current fed to the DFBQCL was modulated at 5 or 10 kHz with either a sawtooth or triangle wave from a function generator. An example of the output intensity profile is displayed in Fig. 8. As in the room-temperature static cell measurements, the resolved line shape profiles were fit to Voigt profiles with the $\nu_{0,i}$, A_i, and $\Delta\nu_{c,i}$ as best-fit parameters. Additionally, the Voigt profile fitting routine slightly scaled the incident intensity profiles (0.99-0.999) to improve the fits and account for any changes in signal due to beam steering or other effects. Above 1500 K, weaker hot band ($v" > 0$) transitions became observable (right panel Fig. 5), and when present, Voigt profiles were also fit to these additional transitions. From the best-fit parameters, the line strength and collision broadening coefficient can be determined from Eqs. (2) and (6), respectively. Fig. 7 displays the measured line strengths of the R(41.5) and R(42.5) transitions as a function of temperature. Keeping the lower state energy constant, the data was fit to Eq. (4), and the best-fit ref-

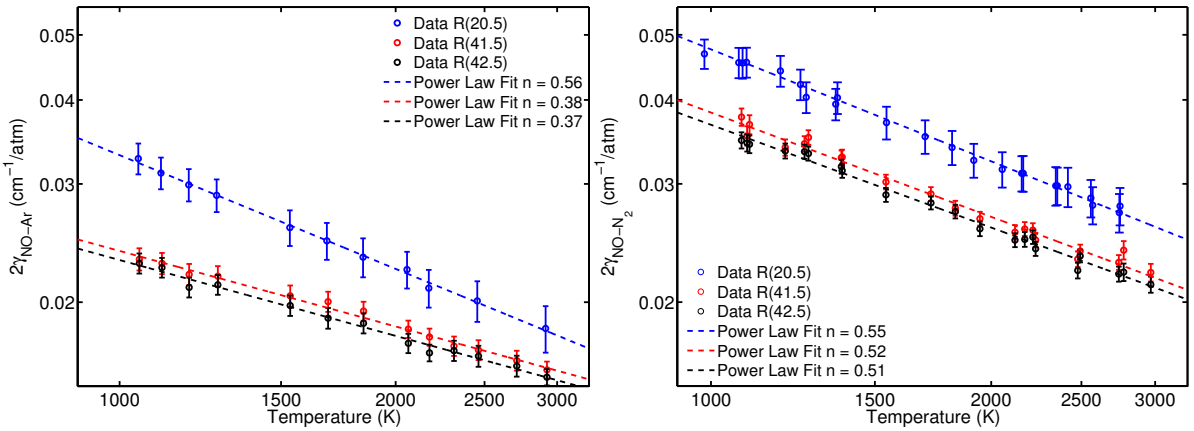

Fig. 6: Measured collision broadening coefficients of NO in Ar and N_2 from 1000 to 3000 K and between 1 and 5 atmospheres.

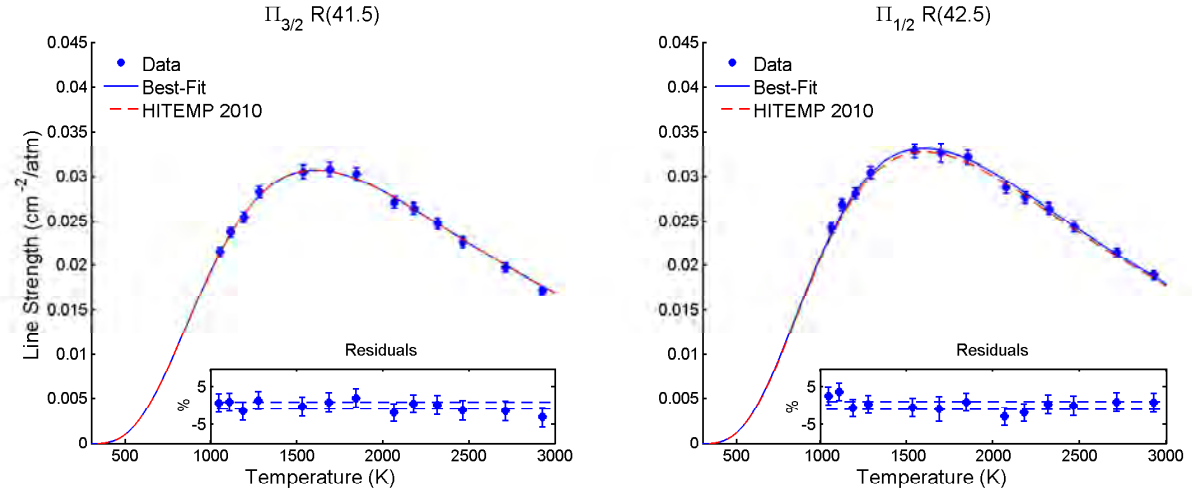

Fig. 7: Measured line strength values of the $\Pi_{3/2}$ R(41.5) and $\Pi_{1/2}$ R(42.5) transitions from NO in Ar shock tube experiments.

erence line strengths, $S_i(T_0 = 296K)$, were found to agree extremely well with the reference line strengths listed in HITEMP 2010. Fig. 6 shows the collision broadening measurements as a function of temperature for the nitrogen and argon mixtures, respectively. The best-fit temperature exponents of the pressure broadening coefficients of the the $\Pi_{3/2}$ R(41.5) and $\Pi_{1/2}$ R(42.5) transitions in argon were found to be 0.38 and 0.37, respectively, with $2\gamma_{NO-Ar}(T_0 = 1000K) = 0.0239$ and 0.0231 cm^{-1}/atm. In nitrogen, the collision broadening temperature exponents were found to be 0.52 and 0.51, respectively, with $2\gamma_{NO-N_2}(T_0 = 1000K) = 0.0384$ and 0.0368 cm^{-1}/atm. As the case for the R(20.5) transition, the collision broadening due to Ar was observed to be $\sim$ 37% smaller than N_2 induced broadening. For convenience, all measured spectroscopic parameters are summarized and compared to HITEMP 2010 values in Tables 1 and 2. A discussion of the uncertainty anaylsis for these measurements can be found in the Appendix.

5. Sensor Demonstration

5.1. Temperature Measurements in Non-reacting Shock-heated Gas

The utility of the studied NO transitions is demonstrated through temperature measurements during shock tube experiments over a wide range of temperatures. Most temperature measurements were made during experiments with NO mole fraction fixed, but an NO formation experiment that demonstrated the sensor's ability to measure temperature during species transients is presented in the next section. Examples of measured pressure and light transmission data are shown in Fig. 8 and in the top panel of Fig. 10. For fixed-NO experiments, the gas mixture was either 1.97% NO in N_2 or 2% NO in Ar. The first step in the pressure trace represents a nearly instantaneous jump in pressure and temperature of the test gas mixture resulting from the passing of the incident shock over the measurement location. The increases in temperature and pressure from the incident shock results in a decrease in the fixed-DA signal from the ECQCL, which

Table 2: Comparison of measured collision broadening parameters for NO with HITEMP 2010. Uncertainties are in parenthesis and represent the statistical uncertainties from the best-fit power law except for the static cell measurements at 298.7 K.

ν_0 [cm^{-1}]	Collision Partner	2γ [cm^{-1}/atm]		2γ(1000K)		n	
		Measured (298.7 K)	HITEMP (296 K)	Best-fit	HITEMP	Best-fit	HITEMP
1939.614	[a]N_2	0.101 (1%)	0.0964 (5-10%)		0.0464 (9-18%)		0.6 (10-20%)
1940.778	[a]N_2	0.1045 (1%)	0.0998 (5-10%)	0.0475 (1.1%)	0.0426 (10-20%)	0.55 (3.2%)	0.7 (10-20%)
	Ar			0.0331 (1.4%)		0.56 (4.0%)	
1986.537	[a]N_2		0.0900 (5-10%)	0.0384 (2.1%)	0.0384 (Est.)	0.52 (5.9%)	0.7 (Est.)
	Ar			0.0239 (1.6%)		0.38 (5.9%)	
1987.10	[a]N_2		0.0900 (5-10%)	0.0368 (1.8%)	0.0434 (Est.)	0.51 (4.9%)	0.6 (Est.)
	Ar			0.0231 (1.9%)		0.37 (7.3%)	

[a] Listed HITEMP 2010 2γ values are adjusted for air (79% N_2, 21% O_2)

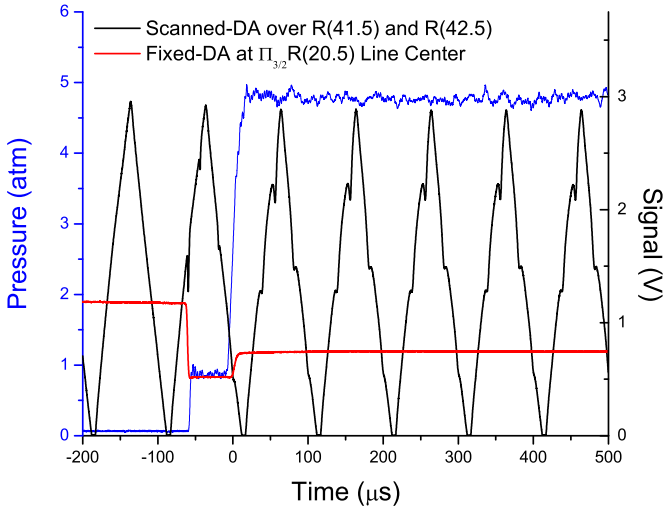

Fig. 8: Measurement traces from reflected shock tube experiment of 1.97% NO in N_2. T_5 = 1550 K and P_5 = 4.8 atm.

corresponds to a decrease in transmitted light and thus more absorbance. Approximately 50μs later, another rise in pressure is observed, resulting from the passing of the reflected shock over the measurement location. The additional jump in pressure and temperature result in an increase of light transmission and thus a decrease in absorbance. The 10 kHz scanned-DA signal from the DFBQCL with dips in signal due to the R(41.5) and R(42.5) transitions can also be observed. During experiments with mixtures of NO in N_2, it is evident from the rolling off of the pressure trace that the jump after the reflected shock is not nearly as instantaneous as the jump after the incident shock. This is the result of shock-bifurcation that is a phenomenon observed in shock tube experiments containing mostly diatomic or polyatomic molecules [38, 39]. However, effects of shock-bifurcation are not present during experiments performed with Ar-balanced mixtures. Another carefully considered phenomenon in the shock tube experiments was vibrational relaxation. Vibrational relaxation is an extensively studied subject regarding the time-lag required for the vibrational energy states of a gas to reach an equilibrium distribution after an instantaneous change in thermodynamic conditions. Works by Taylor *et al.* and Wray provide adequate characterization of vibrational relaxation phenomena for our purposes. Of note is that vibrational relaxation times of mixtures of NO in argon are significantly shorter than for mixtures of NO in nitrogen [40, 41], so vibrational relaxation was considered for only the shock-heated NO in nitrogen mixtures. Using the pressure traces, characteristic total relaxation times (e.g. vibrational relaxation time of 2% NO in N_2 at 2000 K and 1 atm $\sim 60\mu s$), and fixed-DA absorbance traces, it was possible to determine when the vibrational energy distribution could be assumed to be in equilibrium. Furthermore, the temperature measurements presented below provide confidence that the method used to account for vibrational relaxation was adequate.

Temperature measurements during the fixed-NO experiments are displayed in Fig. 9. To convert absorbance data into temperature measurements, the ratio of the $\Pi_{3/2}$R(20.5) transition's absorbance and the $\Pi_{3/2}$R(41.5) (or $\Pi_{1/2}$R(42.5)) transition's integrated absorbance was utilized. This ratio can be shown to be approximately a function of only temperature and pressure if the temperature dependence of the line shape is known

$$R = \frac{\alpha(R(20.5))}{A(R(41.5\ or\ 42.5))} = \frac{S_1(T)\Phi_1(\nu_{0,1})}{S_2(T)} \approx f(T,P) \quad (8)$$

It should be noted that due to the presence of the line shape function in the ratio, there is a slight dependence on collision partner concentration, but if there is only one primary collision partner, as is the case for these measurements, then Φ_i becomes a function of pressure and temperature. Temperature is determined through an iteration loop that converges on a temperature once the simulated ratio of absorbance and integrated absorbance matches the measured ratio value. Known temperatures are determined from the measured shock speed and the normal-shock relations which provide accurately known conditions within $\sim 1\%$ [23]. The error bars in the measurements receive contributions from the uncertainties in $2\gamma_{NO-N_2/Ar}$ of the R(20.5) transitions measured in the previous section, line strengths, the measured ratio of absorbance to integrated absorbance, and – at elevated temperatures – the output wavelength of the ECQCL. At elevated temperatures the line shape profile narrows, increasing the

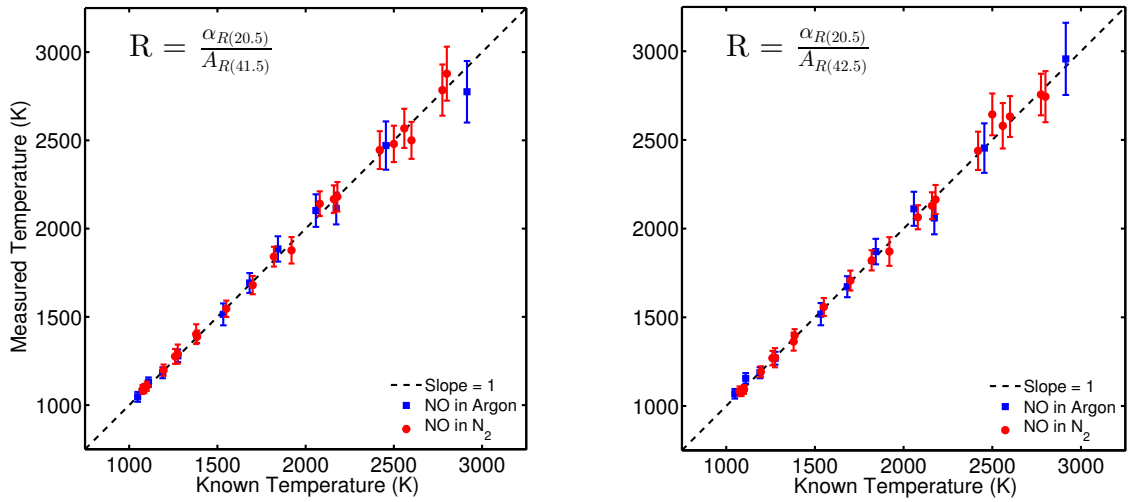

Fig. 9: Demonstration of temperature measurement for fixed concentrations of NO in Ar and N_2. The left panel displays temperature values obtained from the ratio of R(20.5) line center absorbance and R(41.5) integrated area, and the right panel displays temperature values obtained from the ratio of R(20.5) line center absorbance and R(42.5) integrated are.

significance of the uncertainty in output wavelength. Furthermore, the simulations shown in Fig. 3 indicate that the temperature sensitivity of the sensor is best below 2000 K, which is supported by the reduced scatter in measurements made below 2000 K. Despite the temperature sensor's increased uncertainty at temperatures above 2000 K, known and measured temperatures show good agreement. Differences between measured and known temperatures are demonstrated to be at most 5% but typically less than 2%. While temperature measurements from both ratios display similar accuracy and precision, the R(20.5)/R(41.5) scheme is recommended due to a larger ΔE".

5.2. Temperature and NO Species Measurements During NO Formation

A final demonstration is shown in Fig. 10 to highlight the capability of the sensor to measure species at high-bandwidth and temperature in non-equilibrium conditions. Here, NO was formed from 1.3% NO_2 in Ar during a shock tube experiment. The top panel of Fig. 10 shows the pressure trace and the recorded signals from the IR-detectors. The bottom panel shows NO mole fraction and temperature measurements along with the results from a constant-volume chemical kinetic simulation (Chemkin and GRIMech 3.0 [42]) at the experimental post-reflected shock conditions. Temperature measurements were made using the ratio of Eq. (8) as previously explained, and provide an independent check on the non-reactive data set. From the measured temperature, NO mole fraction can be calculated from the measured spectroscopic parameters and Eqs. (1) or (2). Temperature and NO mole fraction measurements show good agreement with the kinetic simulation with differences between measured and simulated temperature being less than 3.5% and differences between measured and simulated mole fraction being less than 4%.

6. Summary and Conclusions

Absorption transitions in the fundamental vibration band of nitric oxide were identified for two-color thermometry and species sensing in high-temperature applications. The R(20.5) transitions near 1940 cm^{-1} and the R(41.5) and R(42.5) transitions near 1987 cm^{-1} were selected for their large lower state energy difference and relative isolation from water vapor. The R(20.5) transitions were accessed by an external-cavity quantum cascade laser while the R(41.5) and R(42.5) transitions were accessed by a distributed-feedback quantum cascade laser. Spectroscopy experiments were performed in a room-temperature static cell and in shock tube experiments with conditions from 1000 to 3000 K and 1 to 5 atm. Compared to the HITEMP database, our measured transition line strengths were found to be in good agreement but with reduced uncertainties. Furthermore, room-temperature collision broadening coefficients of NO in N_2 for the R(20.5) transitions were measured to be within 5% of the reported HITEMP value of pressure broadening in air but within 1% of similar room-temperature measurements of pressure broadening in N_2. The temperature dependence of the collision broadening for NO in N_2 was found to be considerably different from the values reported in HITEMP which was expected given the lack of high-temperature data for the transitions selected and the inadequacy of the power-law. Additionally, new spectroscopic data including collision broadening of the NO transitions in argon was characterized for high temperatures. The sensing capabilities of the studied transitions were demonstrated by measuring temperature in fixed-NO shock tube experiments spanning 1000 to 3000 K and by measuring temperature and NO mole fraction during an NO formation experiment at 1700 K, proving the sensor's capabilities in non-equilibrium conditions. The

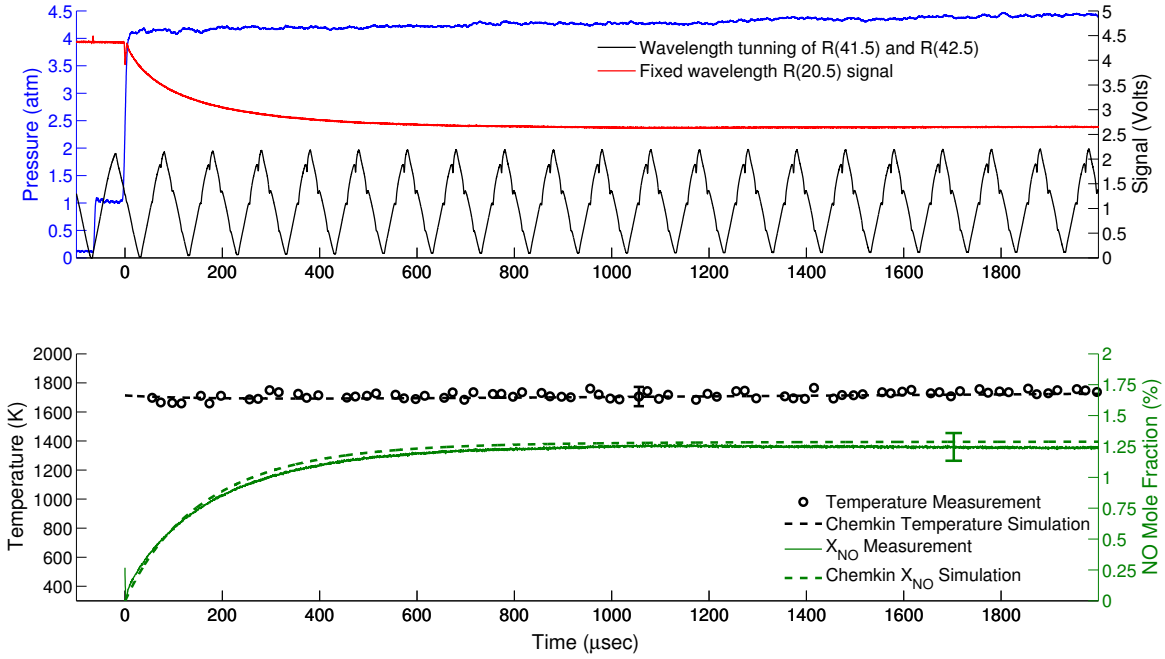

Fig. 10: Demonstration of temperature and NO measurements during an NO formation experiment. Conditions at the beginning of Region 5: 1.3% NO_2 in argon at 1714 K and 4.15 atm.

sensor demonstration provided accurate measurements of temperature from 1000-3000 K and during transient NO conditions.

Acknowledgments

This work was supported by the Air Force Office of Scientific Research through AFOSR Grant No. FA9550-15-1-0049, with with Dr. Michael Kendra as program manager. The authors would like to thank Julian Girard for his assistance in equipment setup.

Appendix: Uncertainty Analysis of Spectroscopic Measurements

Uncertainty analysis was performed for individual data points and for the temperature dependent data, S and 2γ, via regression analysis. The error bars of individual data points in Figures 6 and 7 are calculated by addition in quadrature of the uncertainty contributors listed below. Uncertainties of room-temperature static cell measurements of 2γ and S listed in Tables 1 and 2 were also calculated by addition in quadrature. The reported uncertainties of the values in Tables 1 and 2 for best-fit R(41.5) and R(42.5) $S(T_0)$ and best-fit $2\gamma(1000K)$ and n were determined from regression analysis of their respective data sets over the 1000 – 3000 K temperature range.

For the scanned-DA experiments, contributors to uncertainty of individual S and 2γ data points include uncertainties in:

i. Temperature, T:
   (a) Room-temperature static cell experiments: The measurement uncertainty in the sample temperature was 1 K which contributed 1% to uncertainty in line strength at 296 K.
   (b) Shock tube experiments: For the temperature dependent data, uncertainty in temperature affects the uncertainty of the fitting parameters (i.e. $S(T_0)$, $2\gamma(T_0)$, and n). As previously mentioned, thermodynamic conditions behind the reflected shock are known to within $\sim 1\%$.

ii. Pressure, P:
   (a) Room-temperature static cell experiments: The uncertainty in the measured pressure was 0.5% which resulted in contributions of 0.5% to uncertainties in both S and 2γ.
   (b) Shock tube experiments: The pressure uncertainty (in %) from each shock tube experiment contributes the same percent uncertainty to S and 2γ. As previously mentioned, thermodynamic conditions behind the reflected shock are known to within $\sim 1\%$.

iii. NO mole fraction, X_{NO}: The 2% uncertainty in NO mole fraction contributed 2% and $< 0.1\%$ uncertainty in S and 2γ, respectively.

iv. Path length, L:
   (a) Room-temperature static cell experiments: The path length uncertainty of the room-temperature optical cell is 1% which contributed 1% uncertainty in S.

(b) Shock tube experiments: The 15.24 cm path length of the shock tube is well-known and documented in other works using the same facility. Uncertainty in the path length contributed 1% uncertainty to S.

v. Non-linear regression confidence intervals of the best-fit parameters from the Voigt profile fits, A and $\Delta\nu_c$:
   (a) Room-temperature static cell experiments: The confidence intervals of the best-fit parameters contributed 0.06 and 0.09% to uncertainty in S and 2γ, respectively.
   (b) Shock tube experiments: Fitting parameter confidence intervals for the shock tube experiments were much larger due to the increased residuals of the fit as shown in Fig. 5. Uncertainties in A and $\Delta\nu_c$ contributed $\sim 2\%$ uncertainty to S and 2γ, respectively.

vi. NO self-broadening, $2\gamma_{NO-NO}$:
   (a) Room-temperature static cell experiments: The HITEMP 2010 room-temperature $2\gamma_{NO-NO}$ values for the R(20.5) transitions have reported uncertainties of 10-20%. For these measurements, however, uncertainty in $2\gamma_{NO-NO}$ is a small contributor to uncertainty in $2\gamma_{NO-N_2}$ (0.25%) because the mixture is only 1.01% NO by mole fraction.
   (b) Shock tube experiments: NO self-broadening at elevated temperatures is not known for the R(41.5) or R(42.5) transitions, but since the mixtures are only 2% NO, the contribution to uncertainty in $2\gamma_{NO-N_2}$ or $2\gamma_{NO-Ar}$ from uncertainty in $2\gamma_{NO-NO}$ is expected to be low. This was checked by using $2\gamma_{NO-NO}(296K)$ reported in the HITEMP database and assuming a temperature exponent $n_{self} = 0.75$. Furthermore, the uncertainty of both $2\gamma_{NO-NO}(296K)$ and n_{self} were assumed to be 20%. The uncertainty analysis for $2\gamma_{NO-N_2}$ or $2\gamma_{NO-Ar}$ resulted in uncertainty contributions from $2\gamma_{NO-NO}$ of $< 1\%$.

For the fixed-DA measurements of the R(20.5) transition in the shock tube, contributors to uncertainty of inferred 2γ data points were evaluated via perturbation analysis. These contributors included uncertainties in:

i. Temperature, T: As mentioned previously, conditions behind the reflected shock are known to within $\sim 1\%$, but with increasing temperature the nominal uncertainty (in Kelvin) increases, leading to increased uncertainty at elevated temperatures. The contribution to uncertainty of inferred 2γ data points due to temperature uncertainty ranges from 1-3%.

ii. Pressure, P: As mentioned previously, conditions behind the reflected shock are known to within $\sim 1\%$. The contribution to uncertainty of inferred 2γ data points due to pressure uncertainty ranges from 0.1-0.3%.

iii. Absorbance, α: Uncertainty in the measured absorbance is quantified as the standard deviation of the measurement. As the absorbance changes over the temperature range (see Fig. 3), the percent uncertainty in absorbance increases resulting in a range of 0.2 – 2% uncertainty contribution to the inferred 2γ data points.

iv. NO mole fraction, X_{NO}: The mixtures used in these experiments have 2% uncertainty in X_{NO} which results in a 2–2.5% contribution to uncertainty of the inferred 2γ data points.

v. Path length, L: The 15.24 cm path length of the shock tube is well-known and documented in other works using the same facility. The uncertainty contribution to the inferred 2γ data points due to uncertainty in L (1%) is around 0.8% for all experiments.

vi. Laser output frequency, ν: The uncertainty of the wavelength meter cited by the manufacturer (Bristol) is < 0.001 cm^{-1} at 5μm. However, the ECQCL output frequency was found to be slightly unstable. The uncertainty in the frequency was quantified by observing the room temperature absorbance signal prior to experiments. Since the line shape and line strength at room temperature are well-known for the R(20.5) transitions, the absorbance signal observed directly translated to laser frequency uncertainty. This uncertainty was found to be 0.0075 cm^{-1} which resulted in contributions to uncertainty of 0.4-0.8% for the inferred 2γ data points.

vii. Line strength, S: The uncertainty of the R(20.5) line strengths measured during the static cell experiment was found to be 2.5%. This resulted in contributions to uncertainty of 4.2-4.8% for the inferred 2γ data points.

viii. NO self-broadening, $2\gamma_{NO-NO}$: NO self-broadening at elevated temperatures is not known for the R(20.5) transitions, but since the mixtures are only 2% NO, the uncertainty in $2\gamma_{NO-N_2}$ or $2\gamma_{NO-Ar}$ due to uncertainty in $2\gamma_{NO-NO}$ is expected to be low. This was checked by using $2\gamma_{NO-NO}(296K)$ reported in the HITEMP database and assuming a temperature exponent $n_{self} = 0.75$. Furthermore, the uncertainty of both $2\gamma_{NO-NO}(296K)$ and n_{self} were assumed to be 20%. The resulting perturbation analysis for $2\gamma_{NO-N_2}$ or $2\gamma_{NO-Ar}$ resulted in uncertainty contributions of $\sim 0.1\%$ for the inferred 2γ data points.

References

[1] Miller JA, Bowman CT. Mechanism and modeling of nitrogen chemistry in combustion. Progress in Energy and Combustion Science 1989;15(4):287–338. doi:10.1016/0360-1285(89)90017-8.

[2] Haagen-Smit AJ. Chemistry and Physiology of Los Angeles Smog. Industrial and Engineering Chemistry 1952;44(6):1342–1346. doi:10.1021/ie50510a045.

[3] Rothman L, Gordon I, Barber R, Dothe H, Gamache R, Goldman A, et al. HITEMP, the high-temperature molecular spectroscopic database. Journal of Quantitative Spectroscopy and

Radiative Transfer 2010;111(15):2139–2150. doi:10.1016/j.jqsrt.2010.05.001.

[4] Ness TG, Lovejoy RW, Chackerian C. Pressure broadening coefficients of $^{14}N^{16}O$-N_2 gas mixtures. Journal of Molecular Spectroscopy 1987;124:229–235. doi:10.1016/0022-2852(87)90137-8.

[5] Ballard J, Johnston WB, Kerridge BJ, Remedios JJ. Experimental spectral line parameters in the 1-0 band of nitric oxide. Journal of Molecular Spectroscopy 1988;127(1):70–82. doi:10.1016/0022-2852(88)90009-4.

[6] Spencer MN, Chackerian C, Giver LP, Brown L. The nitric oxide fundamental band: frequency and shape parameters for rovibrational lines. Journal of Molecular Spectroscopy 1994;165(2):506–524. doi:10.1006/jmsp.1994.1154.

[7] Coudert L, Dana V, Mandin J, Morillonchapey M, Farrenq R. The spectrum of nitric oxide between 1700 and 2100 cm^{-1}. Journal of Molecular Spectroscopy 1995;172(2):435–448. doi:10.1006/jmsp.1995.1191.

[8] Pope RS, Wolf PJ. Rare gas pressure broadening of the NO fundamental vibrational band. Journal of Molecular Spectroscopy 2001;208:153–160. doi:10.1006/jmsp.2001.8401.

[9] Krauss RH, McDaniel JC. A clean air continuous flow propulsion facility. In: AIAA 17th Aerospace Ground Testing Conference. Nashville, TN; 1992,doi:10.2514/6.1992-3912.

[10] Spearrin RM, Schultz IA, Jeffries JB, Hanson RK. Laser absorption of nitric oxide for thermometry in high-enthalpy air. Measurement Science and Technology 2014;25(12):125103. doi:10.1088/0957-0233/25/12/125103.

[11] Mohamed A, Rosier B, Henry D, Louvet Y, Vargese PL. Tunable diode laser measurements on nitric oxide in a hypersonic wind tunnel. AIAA journal 1996;34(3):494 – 499. doi:10.2514/3.13095.

[12] Hanson RK, Monat JP, Kruger CH. Absorption of CO laser radiation by NO. Journal of Quantitative Spectroscopy and Radiative Transfer 1976;16(8):705–713. doi:10.1016/0022-4073(76)90063-7.

[13] Falcone PK, Hanson RK, Kruger CH. Tunable diode laser absorption measurements of nitric oxide in combustion gases. Combustion Science and Technology 1983;35:81–99. doi:10.1080/00102208308923704.

[14] Falcone PK, Hanson RK, Kruger CH. Tunable diode laser measurements of the band strength and collision halfwidths of nitric oxide. Journal of Quantitative Spectroscopy and Radiative Transfer 1983;29(3):205–221. doi:10.1016/0022-4073(83)90039-0.

[15] von Gersum S, Roth P. IR-diode laser measurements on the decomposition of NO behind shock waves. Experiments in Fluids 1992;13:299–304. doi:10.1007/BF00209501.

[16] Chao X, Jeffries JB, Hanson RK. *In situ* absorption sensor for NO in combustion gases with a 5.2 μm quantum-cascade laser. Proceedings of the Combustion Institute 2011;33(1):725–733. doi:10.1016/j.proci.2010.05.014.

[17] McCurdy MR, Bakhirkin YA, Tittel FK. Quantum cascade laser-based integrated cavity output spectroscopy of exhaled nitric oxide. Applied Physics B: Lasers and Optics 2006;85:445–452. doi:10.1007/s00340-006-2365-0.

[18] Oh DB, Stanton AC. Measurement of nitric oxide with an antimonide diode laser. Applied optics 1997;36(15):3294–3297. doi:10.1364/AO.36.003294.

[19] Mihalcea RM, Baer DS, Hanson RK. A diode-laser absorption sensor system for combustion emission measurements. Measurement Science and Technology 1998;9(3):327–338. doi:10.1088/0957-0233/9/3/004.

[20] Hanson RK. Applications of quantitative laser sensors to kinetics, propulsion and practical energy systems. Proceedings of the Combustion Institute 2011;33(1):1–40. doi:10.1016/j.proci.2010.09.007.

[21] Hanson RK, Spearrin RM, Goldenstein CS. Spectroscopy and optical diagnostics for gases. First ed.; Springer International Publishing; 2016. ISBN 978-3-319-23251-5. doi:10.1007/978-3-319-23252-2.

[22] Hanson RK, Falcone PK. Temperature measurement technique for high-temperature gases using a tunable diode laser. Applied Optics 1978;17(16):2477–2480. doi:10.1364/AO.17.002477.

[23] Herbon JT. Shock tube measurements of CH_3+O_2 kinetics and the heat of formation of the OH radical. Phd dissertation; Stanford University; 2004.

[24] Farooq A, Jeffries JB, Hanson RK. Sensitive detection of temperature behind reflected shock waves using wavelength modulation spectroscopy of CO_2 near 2.7 μm. Applied Physics B 2009;96(1):161–173. doi:10.1007/s00340-009-3446-7.

[25] Spearrin RM, Ren W, Jeffries JB, Hanson RK. Multi-band infrared CO_2 absorption sensor for sensitive temperature and species measurements in high-temperature gases. Applied Physics B 2014;116(4):855–865. doi:10.1007/s00340-014-5772-7.

[26] Mirels H. Boundary layer behind shock or expansion wave moving into stationary fluid. Tech. Rep.; NACA; 1956.

[27] Petersen EL, Hanson RK. An improved turbulent boundary-layer model for shock tubes. In: 31st AIAA Fluid Dynamics Conference & Exhibit. Anaheim, CA; 2001, p. AIAA 2001–2855. doi:10.2514/6.2001-2855.

[28] Davidson DF, Chang AY, Di Rosa MD, Hanson RK. A cw laser absorption diagnostic for methyl radicals. Journal of Quantitative Spectroscopy and Radiative Transfer 1993;49(5):559–571. doi:10.1016/0022-4073(93)90067-R.

[29] Klingbeil AE, Jeffries JB, Hanson RK. Design of a fiber-coupled mid-infrared fuel sensor for pulse detonation engines. AIAA journal 2007;45(4):772–778. doi:10.2514/1.26504.

[30] Kriesel JM, Hagglund GM, Gat N, Spagnolo V, Patimisco P. Spatial mode filtering of mid-infrared (mid-IR) laser beams with hollow core fiber optics. In: Proc. SPIE; vol. 8993. ISBN 9780819499066; 2013,doi:10.1117/12.2040018.

[31] Bledt CM, Kopp DV, Harrington JA, Kino S, Matsuura Y, Kriesel JM. Investigation of tapered silver / silver halide coated hollow glass waveguides for the transmission of CO2 laser radiation. In: Proc. SPIE; vol. 8218. San Francisco. ISBN 9780819488619; 2012, p. 821802. doi:10.1117/12.912201.

[32] Rothman LS, Gordon IE, Babikov Y, Barbe A, Chris Benner D, Bernath PF, et al. The HITRAN2012 molecular spectroscopic database. Journal of Quantitative Spectroscopy and Radiative Transfer 2013;130:4–50. doi:10.1016/j.jqsrt.2013.07.002.

[33] Goldman A, Brown LR, Schoenfeld WG, Spencer MN, Chackerian C, Giver LP, et al. Nitric oxide line parameters: review of 1996 HITRAN update and new results. Journal of Quantitative Spectroscopy and Radiative Transfer 1998;60(5):825–838. doi:10.1016/S0022-4073(98)00085-5.

[34] Chackerian C, Freedman RS, Giver LP, Brown LR. The NO vibrational fundamental band: O_2-broadening coefficients. Journal of Molecular Spectroscopy 1998;192(1):215–219. doi:10.1006/jmsp.1998.7679.

[35] Bonamy J, Robert D, Boulet C. Simplified models for the temperature dependence of linewidths at elevated temperatures and applications to CO broadened by Ar and N_2. Journal of Quantitative Spectroscopy and Radiative Transfer 1984;31(1):23–34. doi:10.1016/0022-4073(84)90046-3.

[36] Hartmann JM, Rosenmann L, Perrin MY, Taine J. Accurate calculated tabulations of CO line broadening by H_2O, N_2, O_2, and CO_2 in the 200-3000 K temperature range. Applied Optics 1988;27(15):3063–3065. doi:10.1364/AO.27.003063.

[37] Rosenmann L, Hartmann JM, Perrin MY, Taine J. Accurate calculated tabulations of IR and Raman CO_2 line broadening by CO_2, H_2O, N_2, O_2 in the 300-2400 K temperature range. Applied optics 1988;27(18):3902–6. doi:10.1364/AO.27.003902.

[38] Sanderson RJ. Interpretation of pressure measurements behind the reflected shock in a rectangular shock tube. AIAA Journal 1969;7(7):1370–1372. doi:10.2514/3.5352.

[39] Petersen EL, Hanson RK. Measurement of reflected-shock bifurcation over a wide range of gas composition and pressure. Shock Waves 2006;15(5):333–340. doi:10.1007/s00193-006-0032-3.

[40] Taylor RL, Camac M, Feinberg RM. Measurements of vibration-vibration coupling in gas mixtures. Symposium (International)

on Combustion 1967;11(1):49–65. doi:10.1016/S0082-0784(67)80133-4.

[41] Wray KL. Shock-tube study of the vibrational relaxation of nitric oxide. The Journal of Chemical Physics 1962;36(10):2597–2603. doi:10.1063/1.1732339.

[42] Smith GP, Golden DM, Frenklach M, Moriarty NW, Eiteneer B, Goldenberg M, et al. GRI-Mech 3.0. 1999. URL: http://www.me.berkeley.edu/gri_mech/.